Copyright © 1974 American Telephone and Telegraph Company
THE BELL SYSTEM TECHNICAL JOURNAL
Vol. 53, No. 3, March 1974
Printed in U.S.A.

Controlled Current Filaments in PNIPN Structures With Application to Magnetic Field Detection

By G. PERSKY and D. J. BARTELINK

(Manuscript received August 20, 1973)

Stable biasing of multiterminal PNIPN structures to support controlled current filaments is proposed. A filament forms when base layer spreading resistance is sufficiently high for lateral base voltage drops to shut off injection at all but a small interior portion of the structure. For elongated parallel stripe emitter-base configurations, application of a magnetic field normal to the current filament and stripe axes results in lateral displacement of the filament which is detectable through a change in the external circuit current flow pattern. This displacement can be significantly larger than that of a single-pass Hall deflection, yielding high sensitivity. Analysis of an ideal model confirms a substantial improvement in performance over that of conventional Hall devices, viz., a manyfold increase in the ratio of short circuit signal current to drive current, similar improvement in signal-to-offset ratio, and controllable high output impedance making large signal voltages available. Solutions for the ideal model are presented for carrier transport in the I region both without and with lateral diffusive spread. It is argued that departures of actual device behavior from this model are not apt to be important. Possible circuit connections and a sample calculation of parameter values for a realizable structure are also given.

I. INTRODUCTION

The purpose of this paper is to show how PNPN structures can be biased stably to support controlled current filaments and to describe a sensitive magnetic field detector utilizing this principle in a PNIPN structure. PNPN devices are widely used as 2-terminal bistable switches[1] and as 3- and 4-terminal controlled switches,[2] and have also been utilized in 4-terminal operation as a linear amplifier.[3] The multiterminal circuit operation of the PNIPN structure described here forces

nearly equal base and emitter currents and thereby suppresses these switching and amplifying effects. Stable filament formation properties are introduced when significant spreading resistance is incorporated in each base layer. For the operating conditions considered, the central junction remains in reverse bias and supports counterflowing confined streams of both electrons and holes. The shape and position of this filament are controlled by fully characterized device and circuit parameters, in contrast with previously reported filamentary instabilities.[4]

Magnetic field sensing is made possible because a magnetic field applied perpendicular to the filament displaces it laterally and thereby produces a signal in the external circuit. The displacement can be many times larger than the Hall displacement of either carrier species for a single transit of the I region. The I region is incorporated in the structure for the purpose of increasing filament length and hence its interaction with the magnetic field. The analysis will show that the sensitivity of the device can markedly exceed that of an ideal Hall effect detector of similar dimensions. Improved sensitivity is permitted because the compensating electron and hole streams prevent the buildup of a net Hall voltage. For moderate magnetic fields, detection is linear, yielding field polarity as well as magnitude. This behavior differs strongly from that of previously reported filamentary magnetic sensors in which detection is related to precipitous disruption of the filament when the field reaches a sufficient magnitude.[5]

Section II explains how stable multiterminal operation of the PNIPN structure can be achieved and how base resistance leads to the formation of a controlled current filament. An intuitive picture of the magnetic response is then developed. Sections III and IV present an analytical treatment of the filament characteristics and the magnetic response, respectively. Two cases are considered, transport in the intrinsic region without lateral spread and with diffusive spread. Section V assesses various effects that may cause actual device behavior to depart from the ideal operation predicted in Sections III and IV, shows possible circuit connections for the device, and presents theoretical performance characteristics for a realizable structure. Section VI summarizes the main features of the analysis. Preliminary experimental results are presented elsewhere.[6]

II. GENERAL CONSIDERATIONS

Figure 1a shows an elementary circuit which causes the emitter currents to equal the base currents in an idealized one-dimensional

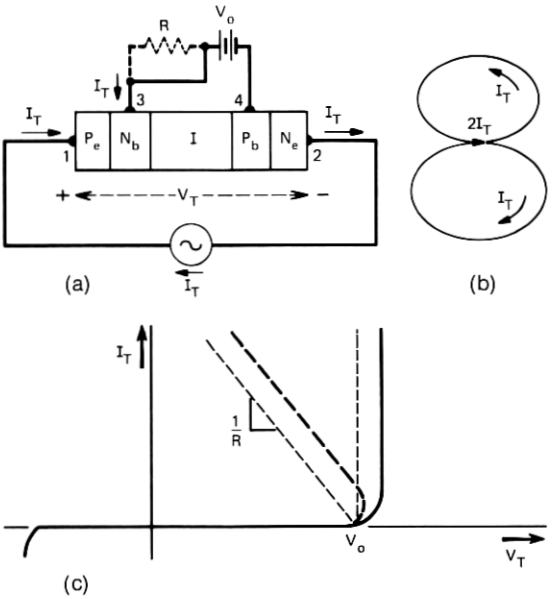

Fig. 1—(a) Four-terminal connection of PNIPN structure. (b) Current loop with figure-8 configuration. (c) Terminal 1–2 $I_T - V_T$ characteristics.

symmetric PNIPN structure with infinite current gain in each emitter-base configuration. We assume in addition that there is no significant recombination in the I region and that electrons and holes have identical properties apart from the charge sign. The current, I_T, supplied by the constant current source in Fig. 1a, follows a figure-8 path as shown in Fig. 1b. Upon entering emitter P_e, the current is injected as hole current through base N_b and region I. It arrives on base P_b where, as a stream of majority carriers, it can exit only through contact 4 to battery V_o. Simultaneously, electrons are injected by emitter N_e to arrive at N_b where, as majority carriers, their only path is to close the loop through contact 3. It is the direct external connection through battery V_o that permits stable conduction of the current $2I_T$ in the I region. Interruption of this external current would force the central junction to become forward biased, corresponding to the "on" state of the switching mode. With battery V_o in place, a typical terminal characteristic between contacts 1 and 2 is shown in Fig. 1c. It is single-valued and consists of the characteristic of a battery V_o and two diodes, all connected in series. Clearly, any finite impedance source connected between these terminals will give dc

stable operation. The fact that stable 4-terminal operation of PNPN devices is possible has recently been demonstrated.[3]

With the addition of a resistance R in series with battery V_o, the voltage across the whole structure is reduced by $I_T R$, causing the characteristic eventually to bend back into a negative resistance region as indicated by the dashed curve in Fig. 1c. Stable operation will then require a source impedance greater than R. Note that this type of voltage turnback is consistent with common-base current gain α maintained at or near unity for each emitter-base configuration, throughout the negative resistance portion of the characteristic except near zero voltage. We have operated a commercial 4-terminal PNPN device, as well as an Ebers equivalent pair of transistors, in this circuit and have observed a stable negative resistance as depicted in Fig. 1c.

Formation of a stable current filament is brought about by base spreading resistance in the otherwise ideal PNIPN structure. The filament formation mechanism can be understood qualitatively with reference to the schematic illustration given in Fig. 2. We retain the assumption that the central diode is everywhere in reverse bias and that $\alpha = 1$ for each emitter-base configuration. This structure is explicitly 2-dimensional, having a stripe geometry, and there is assumed to be no functional dependence on the third coordinate. With the end terminals of each base layer shorted together as shown, the current filament will locate itself along the center line of the structure. We now trace the temporal evolution toward this state, starting from an initial distribution of hole current which is assumed to be uniform. Upon arrival on P_b, the hole current flow is divided between the base

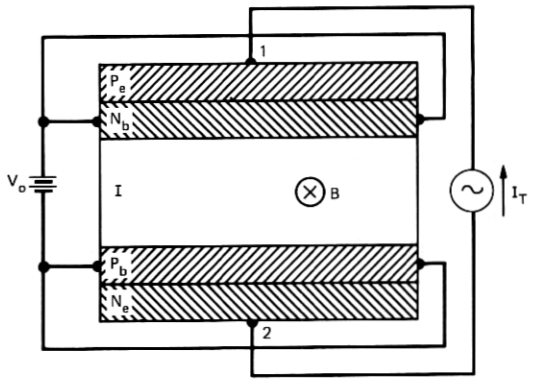

Fig. 2—Filament forming structure with multiterminal circuit connection.

contacts and, consistent with uniform spreading resistance of the base, produces a parabolic voltage profile with its maximum at the center. The total injection of electrons from N_e must correspond to a current I_T, but the base voltage profile will not permit this injection to be uniform. Because the base-emitter voltage is a maximum at the center and because the law governing electron injection is a highly nonlinear function of this voltage, the electron current density will peak sharply at the center. With only moderate lateral spreading in the I region, which is readily attainable,[7] electrons arrive at N_b with a distribution still peaked at the center. Since the average electron must now cross a greater length of resistive base than the average hole did in the uniform distribution, a greater maximum base voltage will be developed and the voltage gradient at points away from the contacts will be enhanced. This sharper voltage profile will in turn lead to an injected hole distribution more sharply peaked than the incident electron distribution. The analysis will show that, after a steady state is reached, the injected distribution of electrons and holes becomes identical. Because of the exponential injection law, this steady-state profile will become progressively sharper as I_T is increased. In particular, when the voltage from base center to base contact is 1 V, the ratio of current density at the center to that at the edge is exp $(qV/kT) \sim e^{40}$. When the filament is highly localized at the center, it is clear that the base resistance acts very much like the resistor R in series with battery V_o in Fig. 1a, and that negative resistance from terminals 1 to 2 in Fig. 2 will similarly result.

The sharpest filament profile occurs when the I region is made extremely thin to eliminate the lateral diffusive and/or space-charge spread. Although a thick I region is needed for good magnetic field sensitivity, previous work on confined electron beams in Si[7] demonstrates that highly localized distributions of electrons and holes arriving at the base layers can still be expected. Accordingly, in this paper it is assumed that space-charge spreading is negligible for reasons of low beam current or electron-hole charge compensation, and diffusion will be used to characterize the lateral spread.

When a magnetic field is applied into the plane of Fig. 2, the filament will move some distance to the right of center, producing an observable current unbalance in the external circuit. Such bodily displacement of the filament is brought about by the Lorentz force, which by virtue of the counterstreaming motion of the electrons and holes causes a Hall displacement to the right for both carrier species. If there were no effects tending to return the filament to center, the interjection of a

unidirectional Hall displacement into each pass of the regenerative particle flow loop would translate the filament indefinitely to the right, in the manner depicted in Fig. 3a.

However, when the filament is shifted off-center, a "restoring force" is produced. This force is proportional to the displacement of the filament from the center, while the Lorentz force remains constant. Therefore, an equilibrium position is attained for which the return injection maximum is displaced back toward center by an amount equaling the single-pass Hall displacement, as indicated in Fig. 3b. Further insight into the nature of this equilibrium state can be gained from a study of Fig. 3c, which illustrates the relationship between the arriving hole current distribution, $J_p(x)$, and voltage profile $V_b(x)$ in base P_b. Since the distribution $J_p(x)$ is displaced to the right of center, it sends more current to the right-hand contact than to the left-hand contact because the resistance is less looking to the right. The point in the $J_p(x)$ profile which divides the leftward from the rightward flowing currents must therefore lie to the left of the centroid of $J_p(x)$.

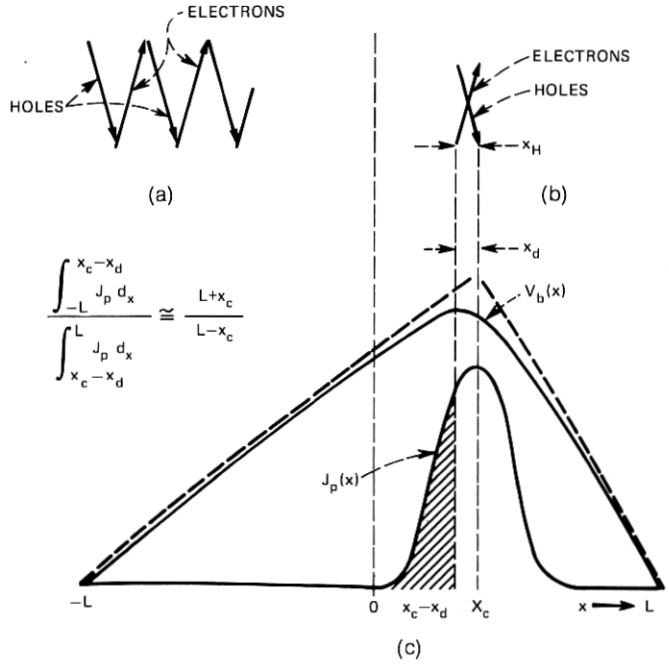

Fig. 3—(a) Representation of multipass displacement in the absence of a restoring force. (b) Representation as in (a) with restoring force. (c) Illustration of relation between hole current profile $J_p(x)$ and base voltage $V_b(x)$ for a displaced filament.

This division point is, of course, the point of maximum base voltage since it is the electric field in the base which causes current conduction toward the contacts. In the vicinity of each contact, far from the filament, the magnitude of the slope of the $V_b(x)$ curve must correspond to the total current at that contact. The ratio of these slopes is, for the present discussion, adequately characterized by the assumption that the straight-line extrapolations intersect at the centroid position x_c, as depicted in the figure, and thus correspond to a ratio $(L + x_c)/(L - x_c)$. The leftward displacement of the maximum of $V_b(x)$ from the $J_p(x)$ centroid is therefore determined by the requirement that the areas under the $J_p(x)$ curve to the right and left of the division point be in the ratio $(L + x_c)/(L - x_c)$. The significance of the leftward displacement x_d is that the return injection profile of the electrons peaks at the voltage maximum and is therefore displaced leftward from the centroid of the arriving distribution by this amount. Equilibrium occurs when x_d is equal to the rightward single-pass Hall displacement x_H.

It is apparent that, to within the above approximations, filament displacement in the magnetic field must be linear since $x_c \propto x_d$ and $x_d = x_H$. Furthermore, the sensitivity increases with drive current because this increase narrows the filament, requiring a larger off-center displacement x_c to bring x_d into equality with x_H. For narrow filaments it is possible for the displacement to be many times larger than x_H, resulting in a signal current greatly exceeding that of a Hall device of similar dimensions. As a practical matter, the short circuit signal current of devices typified by Fig. 2 will saturate at perhaps ten times that of a Hall device, because the sharpness of the profile eventually becomes diffusion-limited. However, this does not appear to be a fundamental limitation on device sensitivity, as is shown by the example at the end of Section IV.

III. DERIVATION OF CURRENT PROFILE AND TERMINAL CHARACTERISTICS IN THE ABSENCE OF A MAGNETIC FIELD

This section presents the calculation of the filament profile in the absence of a magnetic field, as well as the device terminal characteristics. It is shown that the shape of the filament can be characterized directly in terms of the device parameters in both the absence and presence of diffusion. We first consider, in Section 3.1, the highly idealized model introduced in the last section, and neglect diffusion as well. In Section 3.2 we take into account diffusion, which is the most important additional effect present in a real situation.

3.1 Fully regenerative solution

Here we develop the mathematical solution relating the filament current profile to the structure parameters and the drive current I_T. The various voltages and currents entering the analysis are shown in Fig. 4, where it must be remembered that the two contacts on each base are shorted together as in Fig. 3. The procedure followed starts with a consideration of the lower base layer. Employing the continuity equation and the base resistance per unit length, r, we derive a general relation between the hole current per unit length $J_{pi}(x)$ incident on base P_b, and the base voltage $V_b(x)$ developed with respect to the base contacts. From $V_b(x)$ and the terminal voltage V_{eL}, we find the emitter-base voltage profile and, through the junction law, the injected return electron distribution $J_{nr}(x)$. V_{eL} is ultimately determined by the requirement that the total emitter current is I_T. We can write a similar relation, for the upper base, between the incident electron profile $J_{ni}(x)$ and return hole profile $J_{pr}(x)$. In general, the complete set of self-consistent equations is then obtained by introducing the appropriate connection between the incident and return profiles of each species. For a symmetrical structure and in the absence of diffusion, $J_{nr}(x)$ can be directly equated to $J_{pi}(x)$. A single equation immediately results.

The functional dependence of $V_b(x)$ on $J_{pi}(x)$ can be written in the form

$$V_b(x) = \int_{-L}^{L} Z(x, x')J_{pi}(x')dx', \tag{1}$$

where the transfer impedance function $Z(x, x')$ is the voltage response at x to a δ-function of current incident at x'. It is easy to verify that $Z(x, x')$ is given by

$$\begin{aligned} Z(x, x') &= r(L - x)(L + x')/2L, \qquad x \geqq x' \\ &= r(L + x)(L - x')/2L, \qquad x \leqq x'. \end{aligned} \tag{2}$$

The other equations required to complete the description of the lower emitter-base configuration are the voltage balance equation

$$V_e(x) = V_b(x) + V_{eL} \tag{3}$$

and the junction law

$$J_{nr}(x) = J_s \exp [qV_e(x)/kT], \tag{4}$$

where the constant J_s has dimensions of current per unit length. Equation (4) assumes large injection, i.e., net saturation current is

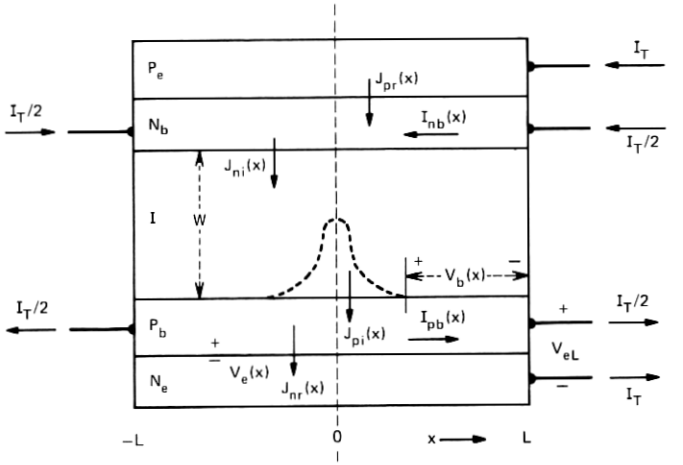

Fig. 4—Definition of variables.

negligible. Although with filamentary conduction this cannot be the case everywhere along the junction, the errors involved are unimportant when high-level injection is achieved in the vicinity of the device center.

Combining Eqs (1) to (4) produces the relation between $J_{pi}(x)$ and $J_{nr}(x)$:

$$I_{\text{reg}} \ln [J_{nr}(x)/J_s] = \int_{-L}^{x} (L - x)(L + x')J_{pi}(x')dx' \frac{1}{2L^2} + \int_{x}^{L} (L + x)(L - x')J_{pi}(x')dx' \frac{1}{2L^2} + \frac{V_{eL}}{rL}, \quad (5)$$

where

$$I_{\text{reg}} \equiv \frac{kT}{qrL} \quad (6)$$

is a structural, regenerative current constant and is the amount of current necessary to produce a voltage drop kT/q when flowing from base center to either base contact. Differentiating (5) yields

$$-\frac{I_{\text{reg}}}{J_{nr}(x)} \frac{dJ_{nr}(x)}{dx} = \frac{1}{2L^2}\left[\int_{-L}^{x} (L + x')J_{pi}(x')dx' - \int_{x}^{L} (L - x')J_{pi}(x')dx'\right], \quad (7)$$

the right-hand side of which may be identified as $1/L$ times the right-

ward flowing current $I_{pb}(x)$ in P_b. Accordingly, we rewrite (7) as

$$-I_{\text{reg}}\frac{dJ_{nr}(x)}{dx} = J_{nr}(x)I_{pb}(x)/L, \tag{8}$$

where

$$\begin{aligned} I_{pb}(x) &= \frac{1}{2L}\left[\int_{-L}^{x}(L+x')J_{pi}(x')dx' - \int_{x}^{L}(L-x')J_{pi}(x')dx'\right] \\ &= \frac{1}{2}\left[\int_{-L}^{x}J_{pi}(x')dx' - \int_{x}^{L}J_{pi}(x')dx' \right. \\ &\qquad \left. + \frac{2}{L}\int_{-L}^{L}x'J_{pi}(x')dx'\right]. \end{aligned} \tag{9}$$

Note that

$$J_{pi}(x) = \frac{dI_{pb}(x)}{dx}. \tag{10}$$

A single equation in one unknown is obtained by invoking the assumptions of symmetry and lack of diffusion:

$$\left.\begin{aligned} J_{ni}(x) &= J_{pi}(x) \\ J_{nr}(x) &= J_{pr}(x) \end{aligned}\right\} \text{ by symmetry,} \tag{11a}$$

$$\left.\begin{aligned} J_{ni}(x) &= J_{nr}(x) \\ J_{pi}(x) &= J_{pr}(x) \end{aligned}\right\} \text{ by diffusion} = 0. \tag{11b}$$

Clearly, all currents are equal. In particular, $J_{nr}(x) = J_{pi}(x)$, so that from (8) and (10) we obtain

$$-I_{\text{reg}}L\frac{d^2I_b(x)}{dx^2} = I_b(x)\frac{dI_b(x)}{dx}. \tag{12}$$

In (12) and thereafter we drop the superfluous subscripts; variable $I_b(x)$ still refers to the rightward flowing current in P_b, and also gives the leftward flowing current in N_b.

The nonlinear second-order differential Eq. (12) can be solved as follows. Rewriting (12) as

$$-2LI_{\text{reg}}\frac{d^2I_b(x)}{dx^2} = \frac{dI_b^2(x)}{dx}$$

and integrating from 0 to x yields

$$-2LI_{\text{reg}}\left[\frac{dI_b(x)}{dx} - \frac{dI_b(0)}{dx}\right] = I_b^2(x) - I_b^2(0). \tag{13}$$

By symmetry about the center line of the structure,

$$I_b(0) = 0. \tag{14}$$

Upon introducing the maximum value of the current profile,

$$J_o \equiv J(0) = \frac{dI_b(0)}{dx}, \tag{15}$$

eq. (13) therefore becomes

$$\frac{dI_b}{dx} = J_0 - \frac{I_b^2}{2LI_{\text{reg}}}. \tag{16}$$

Putting (16) into the form

$$\frac{dI_b}{2LJ_oI_{\text{reg}} - I_b^2} = \frac{dx}{2LI_{\text{reg}}}, \tag{17}$$

and integrating from $-x$ to x results in

$$\frac{1}{\sqrt{2LJ_oI_{\text{reg}}}}\left[\tanh^{-1}\left(\frac{I_b(x)}{\sqrt{2LJ_oI_{\text{reg}}}}\right) - \tanh^{-1}\left(\frac{I_b(-x)}{\sqrt{2LJ_oI_{\text{reg}}}}\right)\right] = \frac{2x}{2LI_{\text{reg}}}. \tag{18}$$

Again, by symmetry about the center line,

$$I_b(-x) = -I_b(x). \tag{19}$$

Using (19) and the property that $\tanh^{-1}(y)$ is an odd function of y, we obtain, after some rearrangement,

$$I_b(x) = \sqrt{2LJ_oI_{\text{reg}}}\tanh\left(\sqrt{\frac{J_oL}{2I_{\text{reg}}}}\cdot\frac{x}{L}\right). \tag{20}$$

From Fig. 4,

$$I_b(L) = \frac{I_T}{2}. \tag{21}$$

Therefore, the current profile peak J_o can be determined from the externally imposed drive current I_T with the relation

$$I_T = 2\sqrt{2LJ_oI_{\text{reg}}}\tanh\left(\sqrt{\frac{J_oL}{2I_{\text{reg}}}}\right). \tag{22}$$

Using this J_o in (20) gives the functional dependence of the base current on position in terms of the drive current and known parameters of the structure. In Fig. 5a, $2I_b(x)/I_T$ is plotted vs. x/L for various values of the dimensionless regeneration parameter $I_T/4I_{\text{reg}}$.

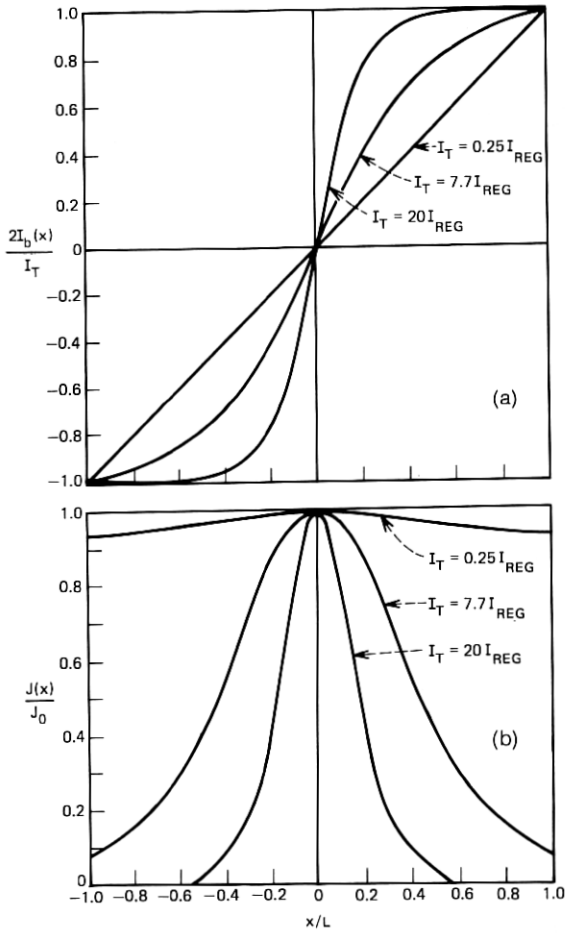

Fig. 5—(a) Position dependence of normalized base current for various values of regeneration parameters. (b) Filament current profile normalized to unity peak value for the same regeneration parameter values as in (a).

For sufficiently large drive currents such that this parameter is much greater than unity, (22) reduces to

$$I_T \approx 2\sqrt{2LJ_oI_{\text{reg}}}, \tag{23}$$

and hence

$$\frac{I_T}{4I_{\text{reg}}} = \frac{qI_T rL}{4kT} \approx \sqrt{\frac{J_oL}{2I_{\text{reg}}}}. \tag{24}$$

Since the right-hand side of (24) is just the argument of the tanh func-

tion in (22), the regeneration parameter is properly approximated by (24) for contours of which the slope is small in the vicinity of $x = L$, i.e., the filament does not touch the boundaries. The contours are adequately described by

$$I_b(x) \approx \frac{1}{2} I_T \tanh\left(\frac{I_T}{4I_{reg}} \cdot \frac{x}{L}\right), \tag{25}$$

which follows upon substituting (23) into (20).

The filament profile itself is obtained simply by differentiating (20) or, for larger I_T, (25). We find, respectively,

$$J(x) = J_o \operatorname{sech}^2\left(\sqrt{\frac{J_o L}{2I_{reg}}} \cdot \frac{x}{L}\right) \tag{26}$$

$$J(x) = \frac{I_T^2}{8I_{reg}} \operatorname{sech}^2\left(\frac{I_T}{4I_{reg}} \cdot \frac{x}{L}\right). \tag{27}$$

Plots of $J(x)/J_0$ vs. x/L for the values of $I_T/4I_{reg}$ used in Fig. 5a are displayed in Fig. 5b. It is evident that, for large values of the regeneration parameter, highly localized current flow is obtained. Equation (24) shows that this parameter is made large through increase of I_T, r, or L. However, $I_{reg}L$ is independent of L so that from (27) one sees that the absolute width of the filament is unchanged by variations of L for fixed r. For a given I_T the only way to sharpen the filament is to increase r. With a high degree of control, the current path is self-contained within an interior portion of the structure. Confined current flows without benefit of physical nonuniformity and is furthermore independent of overall dimension L. The parameter values necessary to produce a well-localized filament can be realized in a practical structure, as is demonstrated by the example in Section V.

We now proceed to calculate the terminal characteristics. The most straightforward approach consists of relating $J(L)$ to I_T with (26) and (22) and using the junction law (4) to relate $J(L)$ to V_{eL}. Recalling, however, that (4) applies only at high-level injection, which may not be satisfied at $x = L$, a more trustworthy method must be employed. Since (4) is reliable at $x = 0$, we may utilize it to find $V_e(0)$ from J_o, and relate J_o to I_T with (22). Then V_{eL} is determined from (3) and (1), where (26) is used in the integral in (1). It is clear that, whatever the junction law, $J(L)$ follows V_{eL}, as impressed through the voltage balance described above, even if V_{eL} is negative. Hence, with this method the errors in calculating V_{eL} are no greater than those in obtaining J_o and $V_b(0)$ with the large injection assumption. When J_o greatly exceeds the saturation current, these errors are small.

From (3) and (4),

$$V_{eL} = \frac{kT}{q} \ln (J_o/J_s) - V_b(0), \tag{28}$$

where, in accordance with (1),

$$V_b(0) = \int_{-L}^{L} Z(0, x')J(x')dx'. \tag{29}$$

Substitution of (2) and (26) into (29) yields

$$\begin{aligned} V_b(0) &= \frac{1}{2} J_o r \int_{-L}^{0} (L + x') \operatorname{sech}^2 \left(\sqrt{\frac{J_0 L}{2I_{\text{reg}}}} \cdot \frac{x'}{L} \right) dx' \\ &\quad + \frac{1}{2} J_o r \int_{0}^{L} (L - x') \operatorname{sech}^2 \left(\sqrt{\frac{J_0 L}{2I_{\text{reg}}}} \cdot \frac{x'}{L} \right) dx' \\ &= J_o r \int_{0}^{L} (L - x') \operatorname{sech}^2 \left(\sqrt{\frac{J_o L}{2I_{\text{reg}}}} \cdot \frac{x'}{L} \right) dx' \\ &= 2 \frac{kT}{q} \ln \cosh \left(\sqrt{\frac{J_o L}{2I_{\text{reg}}}} \right). \end{aligned} \tag{30}$$

Substitution into (28) results in

$$V_{eL} = \frac{kT}{q} \ln (J_o/J_s) - \frac{2kT}{q} \ln \cosh \left(\sqrt{\frac{J_o L}{2I_{\text{reg}}}} \right), \tag{31}$$

where the definition (6) of I_{reg} was used. From (31)

$$V_{eL} = \frac{kT}{q} \ln \left[J_o \Big/ J_s \cosh^2 \sqrt{\frac{J_o L}{2I_{\text{reg}}}} \right]. \tag{32}$$

Together with (22), (32) specifies the terminal characteristics. It is usually reliable only for $J_o \gg J_s$ because of the large injection assumption. When the regeneration parameter is large, (23) may be introduced into (32), yielding V_{eL} directly in terms of I_T.

$$V_{eL} = \frac{2kT}{q} \ln \left[I_T \Big/ 2\sqrt{2LJ_s I_{\text{reg}}} \cosh \left(\frac{I_T}{4I_{\text{reg}}} \right) \right]. \tag{33}$$

The terminal voltage V_T developed by current source I_T, as in Fig. 1c, is

$$\begin{aligned} V_T &= V_o + V_{\text{built-in}} + 2V_{eL} \\ &= V_o + V_{\text{built-in}} + \frac{4kT}{q} \ln \left[I_T \Big/ 2\sqrt{2LJ_s I_{\text{reg}}} \cosh \left(\frac{I_T}{4I_{\text{reg}}} \right) \right]. \end{aligned} \tag{34}$$

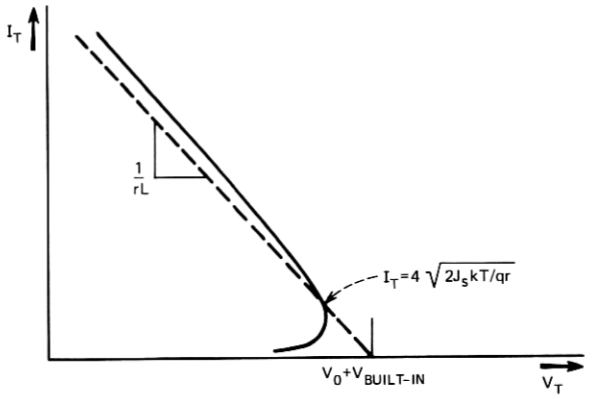

Fig. 6—Form of terminal $I_T - V_T$ characteristic based on fully regenerative solution.

For large argument the cosh function can be approximated by an exponential, permitting (34) to be rewritten as

$$V_T = V_o + V_{\text{built-in}} + \frac{4kT}{q} \ln \left[\frac{I_T}{4\sqrt{2J_s kT/qr}} \right] - rLI_T. \qquad (35)$$

The I_T vs V_T characteristic is displayed in Fig. 6. It should be observed that the asymptotic negative resistance is essentially the same as in the structure of Fig. 1. This is evidence of the fact that, with large regeneration and a filament strongly confined to the center of the structure, regions of the base away from the filament have an effect indistinguishable from external series resistors.

3.2 Diffusion limited solution

While the regenerative solution of Section 3.2 may well be applicable to PNPN structures with a narrow central junction, we must take into account the diffusive spread of the carrier streams in the wide I region of a PNIPN magnetic field sensor. In the presence of diffusion, eqs. (8) and (9) are still valid, but the equality (11b) between the incident and return currents no longer holds. For example, the stream of holes $J_{pr}(x)$ injected by emitter P_e spreads under the action of diffusion while crossing the I region, to arrive at P_b with a new broader profile $J_{pi}(x)$. An initially spike-like or Gaussian profile arrives as a Gaussian, and any other localized distribution also tends toward a

Gaussian. This relation can be expressed mathematically by

$$J_{pi}(x) = \int_{-L}^{L} G(x, x')J_{pr}(x')dx', \tag{36}$$

where $G(x, x')$ is the diffusion Green's function[8]

$$G(x, x') = \frac{\alpha_D}{\sqrt{\pi}} \exp\left[-\alpha_D^2(x - x')^2\right] \tag{37}$$

and α_D is the diffusive spreading parameter. Here α_D is given by

$$\alpha_D^2 \equiv v_d/4D_\perp W, \tag{38}$$

where W is the I region width and v_d and $D_\perp$ are the drift velocity and transverse diffusion coefficient of the carriers traversing it. It is, of course, assumed here that the diffusive spread is insufficient to cause the carrier stream to contact the boundaries at $x = \pm L$.

Utilizing the symmetry relations (11a) and substituting (36) into (9), we obtain from (8) the equation in one unknown, $J_r(x)$,

$$-I_{\text{reg}} \frac{dJ_r(x)}{dx} = \frac{1}{2L^2} J_r(x) \left[\int_{-L}^{x} (L + x')dx' \int_{-L}^{L} G(x', x'')J_r(x'')dx'' - \int_{x}^{L} (L - x')dx' \int_{-L}^{L} G(x', x'')J_r(x'')dx'' \right], \tag{39}$$

where the species subscript has been dropped. In view of the complexity of (39), we attempt only an approximate solution. It is evident that such a solution would be most difficult in the parameter range for which the diffusive spread and regenerative filament width are comparable. In the limit of small diffusion, which we shall not consider, perturbation theory could be used to find the slight modification produced in the completely regenerative solution. At the other extreme, large diffusion, the regenerative mechanism is largely interrupted and the incident current profile tends toward a diffusion-controlled Gaussian.

In the case of large diffusion, where the incident current profile is Gaussian, we may solve (39) approximately by also parameterizing $J_r(x)$ as a Gaussian, but with a different spreading parameter. This procedure can be justified in the following way. If we had a uniform incident current profile, the base voltage developed would be a parabolic function of x. Then, with the assumed exponential junction law, the injected return current is fortuitously Gaussian. This return profile will remain Gaussian whatever the form of $J_i(x)$ in the regions external to $J_r(x)$, as long as $J_i(x)$ is reasonably uniform within the region of

$J_r(x)$. Therefore, in situations where the return profile is much narrower than the incident profile, $J_r(x)$ is always well approximated by a Gaussian. In the diffusion-controlled case, this narrow Gaussian return profile diffusively spreads into the broad Gaussian incident on the opposite base, thereby closing the self-consistent loop.

We assume that

$$J_r(x) = J_o \exp(-\alpha_r^2 x^2) \tag{40}$$

with α_r the return profile spreading parameter. Then, after inserting (40) and (39) into (36), integration yields

$$J_i(x) = \frac{\alpha_D J_o}{\sqrt{\pi}} \int_{-L}^{L} \exp[-\alpha_D^2 (x - x')^2] \exp(-\alpha_r^2 x'^2) dx' \tag{41}$$

$$= \frac{\alpha_i}{\alpha_r} J_o \exp(-\alpha_i^2 x^2),$$

where

$$\alpha_i \equiv \frac{\alpha_r \alpha_D}{\sqrt{\alpha_r^2 + \alpha_D^2}} \tag{42}$$

is the spreading parameter of the incident Gaussian. In performing the integration, it has been assumed that $\alpha_D L \gg 1$ and $\alpha_r L \gg 1$, so the limits may be taken at infinity. We insert the form (41) for (36) into the bracket on the right-hand side of (39) and integrate again. The result is

$$\int_{-L}^{x} (L + x') J_i(x') dx' - \int_{x}^{L} (L - x') J_i(x') dx' = 2L \int_{0}^{x} J_i(x') dx'$$

$$= \frac{\sqrt{\pi} L}{\alpha_r} J_o \operatorname{erf}(\alpha_i x). \tag{43}$$

Substitution of (40) and (43) into (39) yields

$$4 I_{\text{reg}} \alpha_r^3 x = \frac{\sqrt{\pi}}{L} J_o \operatorname{erf}(\alpha_i x), \tag{44}$$

which clearly cannot be satisfied at all x for any spreading parameter values. The necessary approximation consists of replacing the error function by its first-order power series expansion term valid for small $\alpha_i x$. We obtain

$$2 I_{\text{reg}} \alpha_r^3 = \frac{J_o}{L} \alpha_i \equiv \frac{J_o}{L} \alpha_r \alpha_o / \sqrt{\alpha_r^2 + \alpha_D^2}. \tag{45}$$

Using the normalization of (40),

$$J_o = \frac{I_T \alpha_r}{\sqrt{\pi}}, \tag{46}$$

(45) becomes

$$\alpha_r^4 + \alpha_D^2\alpha_r^2 - \frac{(I_T\alpha_D/2LI_{\text{reg}})^2}{\pi} = 0, \tag{47}$$

of which the meaningful root is

$$\alpha_r^2 = \frac{I_T\alpha_D}{2LI_{\text{reg}}\sqrt{\pi}}\left[\sqrt{1 + \left(\frac{\alpha_D LI_{\text{reg}}}{\sqrt{\pi}I_T}\right)^2} - \frac{\alpha_D LI_{\text{reg}}}{\sqrt{\pi}I_T}\right]. \tag{48}$$

For (48) to be accurate requires that the return distribution fall to a negligible amplitude at values of x such that the next expansion term in erf $(\alpha_i x)$ beyond the first makes an insignificant contribution in (44). Thus, setting $x = 1/\alpha_r$, for which

$$\text{erf}\left(\frac{\alpha_i}{\alpha_r}\right) = \frac{2}{\sqrt{\pi}}\left(\frac{\alpha_i}{\alpha_r}\right)\left[1 - \left(\frac{\alpha_i}{\alpha_r}\right)^2/3\cdots\right], \tag{49}$$

the criterion is easily seen to be

$$\left(\frac{\alpha_i}{\alpha_r}\right)^2 \ll 3. \tag{50}$$

This is not really very stringent, because it indicates about 3 percent accuracy when the incident distribution is only three times wider than the return distribution. A simpler expression for α_r^2 than (48) may be obtained when the inequality (50) is well satisfied. We may estimate the magnitude of the dimensionless ratio $\alpha_D LI_{\text{reg}}/\sqrt{\pi}I_T$ by applying (50) to (48), together with the relation $\alpha_D \sim \alpha_i$, which follows from (42) and (50) and is used to eliminate α_i. Neglecting the departure from unity of the bracketed expression in (48), we see that there results the condition

$$\frac{\alpha_D LI_{\text{reg}}}{\sqrt{\pi}I_T} \ll \frac{3}{2}. \tag{51}$$

Therefore, in the diffusion-controlled regime, α_r^2 is well approximated by

$$\alpha_r^2 \approx \frac{I_T\alpha_D}{2\sqrt{\pi}LI_{\text{reg}}}. \tag{52}$$

Surprisingly, the Gaussian parameterization of $J_r(x)$ yields a solution which, in the absence of diffusion [$\alpha_D \to \infty$ in (47)], departs only moderately from the fully regenerative solution (27). Figure 7 compares these solutions for the same value of I_T and shows that the Gaussian approximation overestimates the peak amplitude by 28 percent and is correspondingly narrower. Although the Gaussian therefore only

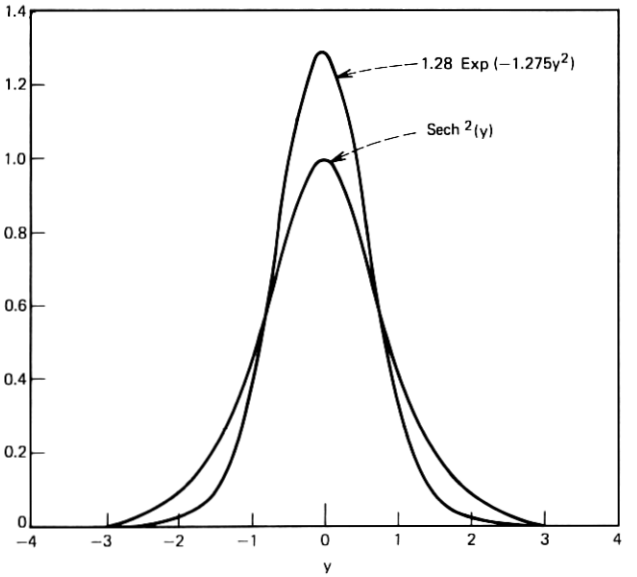

Fig. 7—Comparison of Gaussian approximation in the diffusionless case with fully regenerative solution at one value of I_T.

approximately represents the true solution, it demonstrates that we can carry the large diffusion approximation well outside its intended range of validity without a precipitous drop in accuracy.

The terminal characteristics in the diffusion-controlled case may be found with the same procedure employed for the fully regenerative solution. As long as the diffusion-controlled filament remains narrow compared to $2L$, the asymptotic negative resistance is reduced by the factor $(1 - 1/\sqrt{\pi\alpha_i L})$ which is close to unity.

IV. RESPONSE TO A MAGNETIC FIELD

Section II gave a qualitative explanation of the magnetic response of the PNIPN structure. It was shown that unequal leftward and rightward base currents resulted. Here we calculate this current unbalance in the limit of linear response. We define the signal current I_S as the increase in current flowing out of the right-hand contact of base P_b. Small signal calculation of I_S is simplified because it presupposes that the magnetic driving force is negligibly perturbed by the magnetically produced changes in current profile. Thus, the terminal response is obtained by perturbation theory without a recalculation of the fila-

ment shape. Again, we neglect and consider the effect of diffusion in Sections 4.1 and 4.2, respectively.

4.1 Fully regenerative case

With the magnetic field directed into the page in Fig. 2, both the downward flowing holes and upward flowing electrons are deflected to the right by the Hall displacement

$$x_H = \mu BW, \tag{53}$$

which is the same for both carrier species, assuming equal mobilities. As a consequence of this deflection, relations (11b) become

$$\begin{aligned} J_{ni}(x + x_H) &= J_{nr}(x) \\ J_{pi}(x + x_H) &= J_{pr}(x), \end{aligned} \tag{54}$$

which is applicable as long as the current profiles do not contact the boundaries. The symmetry of the structure preserves relations (11a), which, together with (54), yield from (8) and (9)

$$\begin{aligned} -I_{reg}\frac{d}{dx}J_i(x + x_H) = \frac{1}{2L^2}J_i(x + x_H)\Bigg[\int_{-L}^{x}(L + x')J_i(x')dx' \\ -\int_{x}^{L}(L - x')J_i(x')dx'\Bigg], \end{aligned} \tag{55}$$

where we have dropped the species subscript. By changing variables, (55) can be rewritten

$$\begin{aligned} -I_{reg}\frac{d}{dx}J_i(x) &= \frac{1}{2L^2}J_i(x)\Bigg[\int_{-L}^{x-x_H}(L + x')J_i(x')dx' \\ &\qquad -\int_{x-x_H}^{L}(L - x')J_i(x')dx'\Bigg] \\ &= \frac{1}{2L^2}J_i(x)\Bigg[\int_{-L}^{x}(L + x')J_i(x')dx' \\ &\quad -\int_{x}^{L}(L - x')J_i(x')dx' + 2L\int_{x}^{x-x_H}J_i(x')dx'\Bigg]. \end{aligned} \tag{56}$$

We recognize from (9) that $1/2L$ times the first two terms in the last bracket is $I_b(x)$. The last term, furthermore, can be written to first order in the magnetic field as

$$2L\int_{x}^{x-x_H}J_i(x')dx' \approx -2Lx_HJ_i(x). \tag{57}$$

Therefore, (56) becomes

$$-I_{reg}\frac{d}{dx}J_i(x) = \frac{1}{L}J_i(x)I_b(x) - \frac{x_H}{L}J_i^2(x), \tag{58}$$

which, by (10), can be written

$$-I_{reg}\frac{d}{dx}J_i(x) = \frac{1}{2L}\frac{d}{dx}I_b^2(x) - \frac{x_H}{L}J_i^2(x). \tag{59}$$

Integration of (59) from $-L$ to L, together with the vanishing of $J_i(\pm L)$, yields

$$\tfrac{1}{2}[I_b^2(L) - I_b^2(-L)] = x_H\int_{-L}^{L}J_i^2(x)dx. \tag{60}$$

From the definition of I_S

$$I_b(L) = \frac{I_T}{2} + I_S$$

$$I_b(-L) = -\frac{I_T}{2} + I_S. \tag{61}$$

Therefore, to first order in I_S, (60) becomes

$$\frac{I_S}{I_T} = x_H\int_{-L}^{L}J_i^2(x)dx/I_T^2. \tag{62}$$

Since the right-hand side of (62) is by virtue of x_H already linear in the magnetic field, the unperturbed filament profile may be used for $J_i(x)$. We can see from this equation that I_S/I_T will increase for fixed x_H when the filament profile $J_i(x)$ is made sharper. Evaluation for the fully regenerative profile (27) results in

$$\frac{I_S}{I_T} = \frac{x_H}{12L}\cdot\frac{I_T}{I_{reg}}. \tag{63}$$

Substitution for I_{reg} from (6) and for x_H from (53) gives

$$\frac{I_S}{I_T} = \frac{\mu BW}{2L}\left(\frac{q}{kT}\frac{rLI_T}{6}\right)$$

$$\approx \frac{\mu BW}{2L}\cdot\left(\frac{qV_b(0)}{3kT}\right), \tag{64}$$

where $\mu BW/2L$ is the short circuit current ratio of an ideal Hall device of similar dimensions and $qV_b(0)/3kT$ is a convenient measure of the enhancement of the sensitivity with regeneration. $V_b(0) \approx rLI_T/2$ is the center-to-edge base voltage in the absence of the

magnetic field and can be on the order of volts, leading to enhancement factors in the range 10 to 100.

4.2 Diffusion limited case

Putting (9) into (8) and using only the symmetry relation (11a) we have, upon dropping the species subscripts,

$$-I_{\text{reg}}\frac{d}{dx}J_r(x) = J_r(x)\frac{1}{2L^2}\left[\int_{-L}^{x}(L+x')J_i(x')dx' - \int_{x}^{L}(L-x')J_i(x')dx'\right]. \quad (65)$$

In contrast with the procedure followed in Section 4.1, it is convenient here to integrate (65) from $-L$ to $+L$ at once, to obtain

$$0 = \int_{L}^{L}J_r(x)d\int_{-L}^{x}(L+x')J_i(x')dx' - \int_{-L}^{L}J_r(x)dx\int_{x}^{L}(L-x')J_i(x')dx'. \quad (66)$$

Again, we have assumed the vanishing of the filament profile at the boundaries, i.e., $J_r(\pm L) = 0$. Upon introducing $I_e(x)$ defined by

$$J_r(x) = \frac{dI_e(x)}{dx}, \quad (67)$$

integration by parts of (66) yields

$$0 = [I_e(L) + I_e(-L)]LI_T + [I_e(L) - I_e(-L)] \times \int_{-L}^{L}xJ_i(x)dx - 2L\int_{-L}^{L}I_e(x)J_i(x)dx. \quad (68)$$

From the second form of (9) and from (61)

$$\frac{2}{L}\int_{-L}^{L}xJ_i(x)dx = I_b(L) + I_b(-L) = 2I_S. \quad (69)$$

In analogy with (61), we define I'_S by

$$I_e(\pm L) = \pm\frac{I_T}{2} + I'_S. \quad (70)$$

I_e is a construct which can be interpreted as the lateral emitter current if the emitter, like the base, had contacts at $\pm L$. I'_S is the magnetically produced unbalance in I_e. Substitution of (69) and (70) into

(68) results in

$$0 = I_T I_S' + I_T I_S - \int_{-L}^{L} I_e(x) J_i(x) dx. \tag{71}$$

This equation is merely a simplified version of the integral of (65).

To proceed further, it is necessary to introduce explicitly the simultaneous diffusive spreading and lateral magnetic displacement of the carrier stream as it crosses the intrinsic region. Combining (36) and (54) leads to the general relation between J_i and J_r,

$$J_i(x) = \int_{-L}^{L} G(x, x') J_r(x' - x_H) dx', \tag{72}$$

where $G(x, x')$ is the diffusion Green's function (37). Expanding (72) to first order in x_H yields

$$\begin{aligned} J_i(x) &\approx \int_{-L}^{L} G(x, x') J_r(x') dx' - x_H \int_{-L}^{L} G(x, x') \frac{d}{dx} J_r(x') dx' \\ &= \int_{-L}^{L} G(x, x') J_r(x') dx' - x_H \int_{-L}^{L} \frac{d}{dx} G(x, x') J_r(x') dx', \end{aligned} \tag{73}$$

where the second form has been obtained through an integration by parts with the boundary condition $J(\pm L) = 0$, and the relation $dG/dx' = -dG/dx$. Upon substituting (73) into the integral in (71), the first term of (73) gives rise to an integral of the form

$$g = \int_{-L}^{L} I_e(x) dx \int_{-L}^{L} G(x, x') J_r(x') dx'. \tag{74}$$

It is possible to show by successive integration by parts that

$$g = I_e(L) \int_{-L}^{L} I_e(x) G(x, L) dx - I_e(-L) \int_{-L}^{L} I_e(x) G(x, -L) dx. \tag{75}$$

The vanishing of J_r in the vicinity of the boundaries corresponds to a nearly constant value of $I_e(x)$ in the boundary regions where $G(x, \pm L)$ has a significant magnitude. By noting the normalization

$$\int_{-L}^{L} G(x, \pm L) dx = \frac{1}{2}, \tag{76}$$

we obtain

$$\begin{aligned} g &= \tfrac{1}{2}[I_e^2(L) - I_e^2(-L)] \\ &= I_T I_S'. \end{aligned} \tag{77}$$

Therefore, substitution of (73) into (71) eliminates the I_S' term, leaving

$$I_T I_S = -x_H \int_{-L}^{L} I_e(x) dx \int_{-L}^{L} \frac{d}{dx} G(x, x') J_r(x') dx'. \tag{78}$$

Interchanging the order of integration, integrating by parts with respect to x, and utilizing (67) give

$$I_T I_S = -x_H \Big[I_e(L) \int_{-L}^{L} G(L, x') J_r(x') dx' - I_e(-L) \int_{-L}^{L} G(-L, x') J_r(x') dx' - \int_{-L}^{L} \int_{-L}^{L} J_r(x) G(x, x') J_r(x') dx\, dx' \Big]. \quad (79)$$

Because $J_r(x)$ and $G(\pm L, x)$ do not overlap, the first two integrals in (79) vanish, yielding the final result

$$\frac{I_S}{I_T} = x_H \int_{-L}^{L} \int_{-L}^{L} J_r(x) G(x, x') J_r(x') dx\, dx' / I_T^2. \quad (80)$$

In the limit of no diffusion $G(x, x') \to \delta(x - x')$ and (80) reduces to expression (62), but (80) is valid for arbitrary diffusive spreading. For $J_r(x)$ parameterized as a Gaussian according to (40) and using (37) and the normalization (46), (80) becomes

$$\frac{I_S}{I_T} = x_H \cdot 2\alpha_r^2 L I_{\text{reg}} / I_T \sqrt{1 + 2\alpha_D^2/\alpha_r^2}. \quad (81)$$

In the diffusion-controlled regime characterized by α_r^2 as given in (52), the radical in (81) is approximated by unity, and we find

$$\frac{I_S}{I_T} = x_H \alpha_D / \sqrt{\pi} = x_H \sqrt{v_d / 4\pi D_\perp W}. \quad (82)$$

The result (82) can also be obtained from (80) by letting $J_r(x) \to I_T \delta(x)$ for which

$$\frac{I_S}{I_T} = x_H G(0, 0) = x_H \alpha_D / \sqrt{\pi}. \quad (83)$$

The equality of (82) and (83) demonstrates that, in the diffusion-controlled regime in which α_i/α_r need only satisfy (50), the structure nevertheless responds to a magnetic field as if the return current profile were a very sharp spike. The absence of I_T on the right-hand side of (82) indicates that diffusion saturates the magnetic sensitivity and, unlike (63), the signal is now only linearly proportional to the drive current I_T. To compare the diffusion-controlled detector with a Hall effect device, we substitute for x_H from (53), define the voltage

across the I region at the center by

$$V_B = V_o - 2V_b(0), \tag{84}$$

and introduce the transverse noise temperature of the carriers defined by the Einstein relation

$$kT_n = qD_\perp/\mu. \tag{85}$$

Thus (82) becomes

$$\frac{I_S}{I_T} = \frac{\mu BW}{2L}\left(\frac{L}{W}\sqrt{\frac{qV_B}{\pi kT_n}}\right). \tag{86}$$

The expression in parentheses is the sensitivity enhancement factor for this case, which should be compared with (64), derived in the absence of diffusion. Equation (86) shows that the sensitivity of the diffusion-controlled detector is improved by increasing the central bias voltage until carrier heating predominates. At 8 V, the radical has a value of approximately 10 for W sufficiently large that $T_n \sim T$.

Equation (86) seems to suggest that large sensitivity enhancement with respect to Hall devices can be achieved by making L/W very large. This improvement is, however, illusory because it merely creates an unfavorable geometry for the Hall device. A fair comparison is possible when the device configurations are nearly square. Although in this case an enhancement factor involving only qV_B/kT_n is indicated, this should not be construed as an ultimate limitation imposed by diffusion, but rather as a structural limitation. The following example will illustrate how, for fixed W and L, the fully regenerative enhancement factor can be obtained within the constraints imposed by diffusion. An analysis has been carried out for a structure in which the emitters are contacted at $\pm L$ and have resistances per unit length approaching but less than that of the base layers. It has been found that, in the absence of diffusion, emitter resistance broadens the filament but does not diminish its off-center displacement or signal current when a magnetic field is applied. Since a broader filament is less subject to diffusive spreading when diffusion is taken into account, the effect of sufficient emitter resistance is to carry the filament formation and magnetic response out of the diffusion-controlled regime back into the fully regenerative regime. Therefore, the diffusion limit given by (86) would appear to be appropriate only to the structure analyzed in detail, rather than to be fundamental.

V. PRACTICAL MAGNETIC DETECTORS

The previous sections of this paper have established the fundamental principles according to which controlled filaments might be produced

in PNIPN structures and have analyzed their magnetic sensitivity. Certain idealizations were made in order to develop a coherent theory. One purpose of this section is to give at least a preliminary account of the effect of removing these idealizations, so that we may relate the theory to practical devices. Since magnetic response has heretofore been characterized solely in terms of the short circuit signal current I_S, it is also necessary to analyze the behavior of the magnetic detector in an actual circuit which presents a finite impedance to the detector output. Several realizable circuits are considered. Finally, practical design parameters of a particular detector are given and performance predictions are made. Because filament formation in these devices requires that they be biased into the negative resistance range, there may be a tendency for ac instability, notwithstanding their apparent stability at dc. The dependence of oscillatory behavior on parasitics suggests that, at the outset, only experimental resolution of the stability question is feasible.

5.1 Removal of idealizations

The model developed thus far has been based on the explicit assumptions of (1) complete structural and electrical symmetry, (2) high level injection, (3) infinite current gain, and (4) lateral carrier stream spreading in the I region by diffusion only. It has also been implicit in the analysis that it is permissible to neglect the effects of lateral electric fields in the I region, filament position pinning resulting from structural imperfections, and possible modulation of base width and conductivity. While a detailed investigation of all these effects is beyond the scope of this paper, we shall explain why they are not apt to modify greatly the operation described in the previous sections.

In view of the regenerative nature of the filament, the assumption of infinite current gain might appear questionable. In actual fact, it is easily shown that for finite, but reasonably large, values of common emitter current gain β, device performance is only slightly degraded. We consider first the fully regenerative case, i.e., no diffusion. In the absence of a magnetic field we recall from (11a) and (11b) that $J_i(x) = J_r(x)$. When $\beta \to \infty$, the base current, and hence the base voltage $V_{b\infty}(x)$, are produced entirely by $J_i(x)$ as given by (9) and (1), respectively. For finite β, there is an additional base current component produced similarly by a current profile $J_r(x)/\beta (= J_i(x)/\beta)$ which is subtractive, and hence reduces the base voltage drop to $V_b(x) = (1 - 1/\beta)V_{b\infty}(x)$. This voltage reduction is the same as would be caused by retaining infinite β and reducing r from the original value

r_∞ to

$$r = \left(1 - \frac{1}{\beta}\right) r_\infty. \tag{87}$$

Assuming now that an increase in the actual base resistance is made to compensate for this effect, no modification results in the filament profile if the current through the battery is maintained unchanged. To do so with finite β requires an increase in emitter current by a factor $(\beta + 1)/(\beta - 1)$. It is clear that the filament disappears for $\beta < 1$, but that for $\beta \gg 1$ there need only be a small degradation.

In the diffusion-controlled regime there can be additional significant effects of finite β. When the incident profile is much broader than the return profile, we have $J_r(0)/J_i(0) = \alpha_r/\alpha_i > 1$. Therefore, in the vicinity of the origin, the injection process will give rise to subtractive base current components comparable to those produced by $J_i(x)$, unless β is sufficiently larger than α_r/α_i. The presence of such subtractive components lowers the base voltage at the origin, broadening the return profile and self-consistently lowering $J_r(0)$ until $\beta > J_r(0)/J_i(0)$ is suitably satisfied. Clearly, in the diffusion-controlled regime, finite current gain places a limit on the sharpness of the return profile which cannot be improved by increase of base resistance, i.e., $\alpha_r < \beta\alpha_D$ if the approximation of a Gaussian return profile is retained. Because the magnetic sensitivity is only weakly dependent on the return profile width if (50) is satisfied, as shown by the comparison of (82) and (83), it should only be slightly affected by finite current gain as long as $\beta \gg \sqrt{3}$.

We now briefly consider several effects that can modify filament formation and translation through localized departure from the simple theory. Lateral fields in the I region, brought about by the base layer voltage, can cause deflection[9] of the carrier streams not taken into account in the filament analysis. As a result of the symmetry of the two emitter-base configurations, there is electrical symmetry about the plane midway between the bases. Therefore, the electric field streamlines in the I region may converge near midplane, but still connect, in 1-to-1 fashion, points on the two base layers lying equidistant from filament center. Consequently, although the filament may tend to neck in at the center, this effect will not by itself give rise to additional lateral spreading. Similarly, when the filament is displaced off-center by a magnetic field, these lateral fields will not cause a net restoring force toward device center.

Filamentary instabilities characteristically occur at the particular cross-sectional location where breakdown is most easily initiated.[5] We

have shown that in the present controlled filament formation mechanism, nucleation takes place at the center of the structure. It is still possible, however, that at other locations pinning points may exist for the filament because of structural inhomogeneities such as, for example, a locally enhanced injection efficiency. It is convenient to classify such inhomogeneities according to their size relative to the filament width. Large-scale inhomogeneities, which we shall assume to be reasonably weak, should result in only mild distortion of filament shape and position. In using the structure as a magnetic field sensor, this effect would produce a dc "offset voltage," but not otherwise interfere with the magnetic response. On the other hand, intense small-scale parameter fluctuations would provide distinct filament pinning points. However, in the diffusion-controlled regime this effect should be much reduced. Not only does the diffusion introduce an averaging over dimensions larger than the inhomogeneity, but the accompanying interruption of the feedback loop serves to damp down the multipass gain fluctuations. Because of the filament centering force inherent in the simple theory, pinning the filament becomes progressively more difficult at points away from device center. Ultimately, however, the importance of filament pinning will have to be determined experimentally.

In contrast with structurally associated departures from ideal behavior, localized parameter variations may occur self-consistently induced by the filament itself. Under conditions of high current density, transport in the base may be modified by increased base width or conductivity. It is well known that for transistors operated at high currents the base tends to widen. A similar effect here would lead to a decrease in the base resistance per unit length r. When there is a perfectly compensated filament of electrons and holes in the collector, however, one would expect this effect to disappear but, if there is diffusive spread of carrier streams, locally perfect compensation is absent and some base widening may still occur. A similar local decrease in r would result directly from the conductivity modulation produced by the injected carriers. This effect is readily minimized by making the base layer thin, while keeping the same sheet resistance. With a thinner base the minority carrier density for a given current is lower, while majority carrier concentration is higher. In any event, a local reduction in r will broaden the filament, but one would expect the change in shape to be more pronounced than the actual change in width. Similar modification of the filament profile can be anticipated

from the falloff of injection efficiency at extremely high injection levels.[10]

We now examine the assumptions of structural and electrical symmetry. Structural asymmetries, an example of which is an inequality of base resistance, is subject to technological control and can probably be made small. Such asymmetry will invalidate (11a), resulting in inequivalent electron and hole profiles, but if reasonably small it is unlikely to affect the average filament properties or magnetic response. In contrast, the electrical asymmetry is mostly governed by the disparity of the electron and hole mobilities which is not controllable and may be quite large. An immediate and important consequence of such a mobility ratio is inequality of the electron and hole Hall displacements. It might appear that, because of this inequality, a magnetic field would disrupt the filament by pulling apart the electron and hole streams. Indeed, it has been proposed that the magnetic response of a GaAs double injection diode can be explained by such a mechanism.[5] In the present system, this phenomenon may occur at very high magnetic fields but should normally be avoidable, since the filament is broader than the single-pass Hall displacement and there is no strongly nonlinear pinning point. We have made an analysis based on a rigid displacement of the electron and hole current profiles in the fully regenerative case which indicates that no strong disruption is to be expected. The results show that the coordinate difference between centroids of the return distributions is just one-half the difference between their Hall displacements and is therefore much less than the off-center displacement. A quantitative measure of the unbalance can be obtained from the ratio of the unbalance of the signal currents in the two base layers to their average:

$$\frac{I_{Sn} - I_{Sp}}{I_S} = \frac{3I_{\text{reg}}}{I_T}\left(\frac{x_{Hn} - x_{Hp}}{x_H}\right), \tag{88}$$

where I_{Sn} and I_{Sp} are the signal currents in N_b and P_b, x_{Hn} and x_{Hp} are the Hall displacements of electrons and holes, and I_S and x_H are the average signal current and Hall displacement. The factor $I_T/3I_{\text{reg}}$ is recognized from (64) as twice the enhancement factor, and the right-hand side of (88) is therefore much less than unity.

Another effect of the mobility ratio is the destruction of the inherent filament space-charge neutrality, with the result that there will be increased lateral space-charge spreading. Qualitatively, the effects of space-charge spreading are not greatly different from those of diffusion

and therefore the simple diffusion theory should account for its main features. Since, unlike diffusion, space-charge repulsion scales with filament current, it can be minimized by increasing the base resistances so that the necessary base voltage drops can be achieved at low current. Another approach is to use a circuit that equalizes the carrier densities by equating the electron-to-hole emitter current ratio to the mobility ratio, thereby restoring a nearly neutral filament.

5.2 *Magnetic-detector circuit connections*

Up to this point, the response to a magnetic field has been characterized only in terms of a signal current I_S. Here we consider the interconnection of the detector with a finite load impedance. In the circuit of Fig. 2, I_S could have been detected only by a perfect ammeter. Figure 8 shows a straightforward circuit modification which provides terminals for the connection of load resistors, R_L. In the absence of magnetic field, the voltage and current of the six device terminals, and therefore the filament profile, are completely unaltered by the addition of the external resistors R_{ex}, provided battery V_{00} has the value

$$V_{00} = V_0 + I_T R_{ex}. \tag{89}$$

The magnetic response is most easily understood by adopting an alternative view, in which resistors R_{ex} are considered part of extended base layers having total effective resistance $2R_{eff} = 2R_{ex} + 2rL$. If the filament remains sufficiently confined to fall well within the actual device boundaries, the whole configuration behaves as if it has a base of effective length $2L_{eff}$ related to R_{eff} by $2rL_{eff} = 2R_{eff}$, so that

$$L_{eff} = L + \frac{R_{ex}}{r}. \tag{90}$$

When the load terminals are open circuited, i.e., $R_L \to \infty$, the signal current for both the fully regenerative and diffusion-controlled case, given by (63) and (86) respectively, are unchanged by the change from L to L_{eff}. In (63) the product LI_{reg}, and hence I_S, is independent of L by (6), while in (86) I_S is explicitly independent of L as long as battery V_{00} has been increased in accordance with (89). The open circuit voltage V_{L0} is therefore

$$V_{L0} = 2R_{ex}I_S \tag{91}$$

and has the polarity given in Fig. 8(a). When the terminals are short circuited ($R_L = 0$), I_S is still that given by (63) or (86) and now flows

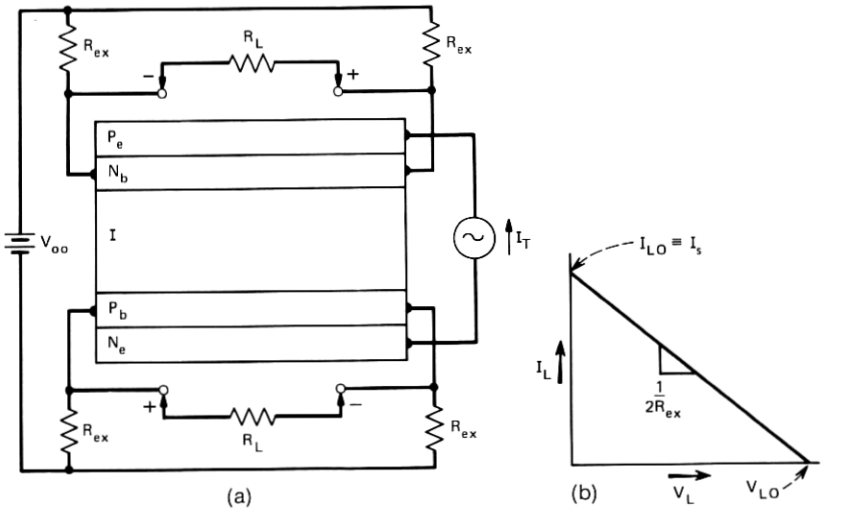

Fig. 8—(a) Magnetic field detector circuit with provision for load R_L. (b) Load line for (a).

completely through the short as I_{L0}. Within the small signal approximation, the device is linear and we obtain the load line given in Fig. 8(b). It is an interesting feature that the output impedance, $2R_{ex}$, is given solely by the magnitude of external resistors. The apparent ability to obtain an indefinite increase in open circuit voltage, by increase of R_{ex}, is just a reflection of the fact that battery V_{00} is correspondingly increased in accordance with (89). It is worth noting that, although I_S has the same value in both the open and short circuited conditions, the off-center displacement of the filament, x_c, is unequal in the ratio L_{eff}/L, reflecting the stronger centering force in the case of the short circuit.

A problem encountered with all magnetic detectors is that structural nonuniformities result in "offset voltages." If the present structure had only a single base layer, the filament would locate itself at the electrical center and there would be no offset voltage. It is expected that in the actual structure the electrical centers of the two base layers will not exactly coincide so that the filament will seek an intermediate position. The result will be an offset voltage for each base layer. It should be clear that the position of this new electrical center is determined only by structural imperfections and will therefore not depend on the enhancement factor. Consequently, the ratio of signal-to-offset voltage for this device should exceed that for the equivalent Hall effect

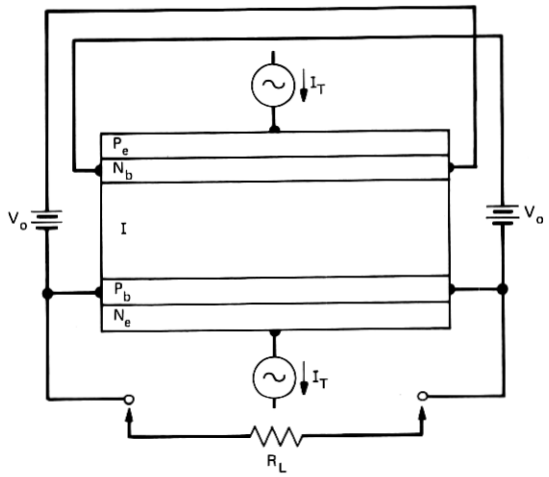

Fig. 9—Signal-summing offset-nulling magnetic detector circuit.

device by this enhancement factor. Furthermore, it is possible to envision a circuit connection, as shown in Fig. 9, in which the signal currents of the two base layers are additive, while their offset voltages are cancelled at least to first order. This circuit has a cross connection of the two base layers by means of two batteries V_o. It also has the interesting feature of displaying terminal characteristics of a nearly ideal magnetically controlled current source $2I_S$.

5.3 Sample device parameters

Figure 10 shows a realizable configuration of the magnetic detector. It is a planar structure formed on a nearly intrinsic substrate. The largest areas are base layers N_b and P_b. Application of reverse bias V_o between N_b and P_b depletes the substrate in the intervening region. Heavily doped emitters N_e and P_e are shaped to be completely on top of the base layers. This structure, with the dimensions shown, can readily be fabricated with current technology and therefore constitutes a reasonable choice for initial experiments. It is also assumed that a base sheet resistance of 10 $k\Omega/\square$ is attainable. With these constraints the structure is far from optimum, but the performance characteristics shown below nevertheless compare favorably with other magnetometers.

With a base sheet resistance of 10 $k\Omega/\square$ and a base width of 12.5 μm, we find a resistance per unit length $r = 800\ \Omega/\mu$m. Equation (6), with $L = 100\ \mu$m, then yields $I_{reg} = 0.312\ \mu$A. For a drive current $I_T = 10$

μA, the filament profile in the fully regenerative case is found from (27) to be

$$J(x) = 0.4 \operatorname{sech}^2\left(8\frac{x}{L}\right) \mu\text{A}/\mu\text{m}. \tag{92}$$

Referring to Fig. 7, the half amplitude points fall at $x_w = \pm 0.85L/8 \simeq \pm 11$ μm, so that the filament is indeed much narrower than the length of the base. Using (30) the corresponding voltage from base center to edge, $V_b(0)$, is 0.366 V. This result may be compared with the value 0.4 V obtained by assuming a perfectly sharp profile for which $I_T/2$ flows through a resistance rL, and indicates that the finite filament width gives rise to a less than 10 percent voltage reduction.

Two considerations enter the choice of the battery voltage V_o. First, it must be sufficient to fully deplete the substrate material between P_b and N_b. Assuming a bulk resistivity of 5 $k\Omega$-cm or better after the necessary processing steps, 5 V would be enough to deplete a plane parallel structure 50 μm across. Allowing for some extra width necessitated by the plane configuration and some margin for being well swept out, a voltage $V_o = 11$ V, corresponding to a drop of ~ 10 V at $x = 0$, should be just adequate. The second consideration is the diffu-

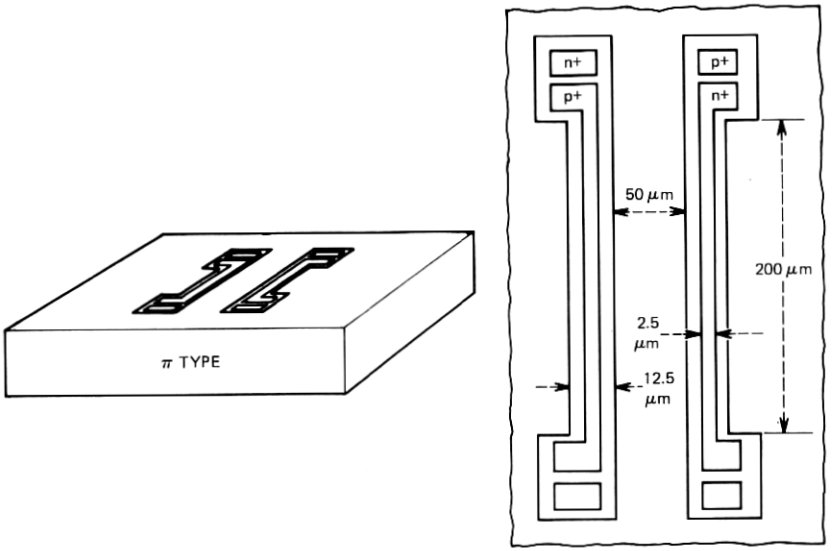

Fig. 10—Illustrative example of realizable magnetic detector.

sive spread. At $x = 0$, the average field in the I region will therefore be in the neighborhood of 2 kV/cm. This field is insufficient to greatly heat the carriers, so that it is justified in (38) to use $D_\perp$ expressed by (85), with $kT_n/q \simeq kT/q = 0.025\ eV$. The resulting value of α_D is 0.2 μm^{-1}, for which the half-amplitude half-width of the Green's function (37) is 4.16 μm. This value is small compared with the value $x_w = \pm 11\ \mu m$ for the filament and works out to an additional spread of only about 12 percent. It is therefore proper to use the fully regenerative solution to calculate the magnetic response.

The regenerative enhancement factor defined in (64) for the above parameters works out to a value of 5. This value only specifies the enhancement of the short circuit signal current I_S over that of an equivalent Hall device. The full available output voltage when the device is used in the circuit of Fig. 8, however, still depends, by (91), on the choice of R_{ex}. Choosing R_{ex} arbitrarily to be 1 MΩ, adjusting V_{00} according to (89), and using (63) and (91) leads to

$$V_{L0} = 22BI_T \text{ volts},$$

which corresponds to a figure of merit of 22 V/GA. This figure of merit is of the same order of magnitude as that reported for other sensitive magnetometers.[11] It is expected that considerable improvement can result from proper design.

VI. SUMMARY

We have shown that spreading resistance in the base layers of a stripe geometry PNIPN structure, with cross section and circuit as shown in Fig. 2, leads to a localized current density profile, i.e., a filament. If lateral spread of the carrier streams in the I region can be neglected, the current density profile is adequately represented by eq. (27). A plot of this function appears in Fig. 5b, which shows that as the drive current I_T is increased, a sharpening of the filament occurs. The relevant parameter is the ratio of I_T to I_{reg}, where I_{reg}, defined in (6), is the amount of base current that would have to flow from device center to a base contact to produce a voltage drop kT/q. The numerical example given in Section V shows that for a realizable structure a typical value of I_{reg} is $\sim 0.3\ \mu A$, so that for $I_T \sim 10\ \mu A$ a highly confined filament is obtained. When carrier transport in the I region is characterized by significant lateral diffusion, the ultimate sharpness of the filament becomes limited. For sufficiently large I_T it becomes a good approximation to represent both the return and incident current density profiles by Gaussians: (40) and (41), respectively. Although,

as shown by (52), the return profile Gaussian continues to narrow with increasing I_T, the incident profile saturates to a width determined solely by diffusion, i.e., for $\alpha_r \to \infty$ we have $\alpha_i \to \alpha_D$, where α_D is given by (38). Using at filament center $v_d = \mu E = \mu V_B/W$ and the definition (85) of the transverse noise temperature, we find $\alpha_D^2 = qV_B/4kT_nW^2$. Therefore, the width of the diffusion controlled filament is independent of parameters characterizing the lateral extent of the structure.

The small signal linear analysis of the magnetic response of the PNIPN structure suggests that it may be regarded as a magnetically controlled current source. The principal result of the paper, eq. (62), relates the magnitude of the magnetic signal current I_S to the drive current I_T, the single-pass Hall deflection x_H, and the incident current density profile in the absence of diffusion. Noting that $I_T/2L$ represents the average current density $\langle J_i(x)\rangle$ and that for any nonuniform function $\langle J_i^2(x)\rangle > \langle J_i(x)\rangle^2$, we see from (62) that I_S/I_T will always be larger than $x_H/2L$, with the inequality increasing for progressively sharper filaments. Since $X_H/2L$ is just the ratio of short circuit signal current to drive current for an ideal Hall detector of dimensions W and $2L$, a clear advantage is indicated. A convenient measure of the enhancement is given by the factor $qV_b(0)/3kT$ in (64), where $V_b(0)$ is the center-to-edge base voltage in the absence of the magnetic field. This factor can be in the range 10 to 100. When lateral diffusion in the I region is important, (80) must be used in place of (62). Equation (80) involves the return profile $J_r(x)$ because $J_i(x)$ is explicitly related to $J_r(x)$ by the diffusion Green's function. The sensitivity enhancement still depends on the sharpness of the current density profile, but now, as shown by (83), an infinitely sharp return profile $J_r(x)$ leads to only a finite enhancement factor, given in (86) in terms of the fundamental parameters. Depending on the device geometry, the enhancement factor can again be of order 10 or more. The parameters which enter it are those pertinent to the diffusion-controlled filament and do not include r or I_T. Although this limiting behavior follows directly from the assumption of an infinitely sharp return profile, the derivation of (82) and subsequent discussion makes clear that it is also descriptive of the sensitivity when the return current profile is only moderately sharper than the diffusion-broadened incident profile. Because, within the limits set forth in Section V, the PNIPN magnetic detector behaves as a magnetically controlled current source, its useful output voltage is determined solely by the circuit in which it is imbedded. For the circuit of Fig. 8, the device considered

in the numerical calculation should have a sensitivity of 22 V/GA when driven at $I_T = 10\mu A$.

An important feature of the PNIPN structure is the possible reduction of the offset level which is so troublesome in magnetic sensors. There are various ways in which this reduction can be effected. Most directly, the offset current, being of geometric origin, is not subject to the enhancement factor experienced by the signal current, and the signal-to-offset ratio is correspondingly improved. Furthermore, the addition of matched external resistors, as in Fig. 8, permits external control of the offset because such resistors act as extensions of the base layers, increasing the effective length of the device and thereby making a percentage improvement in the tolerance. A quite different approach to offset reduction is represented by the circuit of Fig. 9, in which the device incidentally appears to function as a magnetic current source. Analysis indicates that in this circuit configuration the signal currents in the base layers will be summed in R_L, while the offset currents will be nulled to first order, i.e., to the extent that they are of the same magnitude in each base layer. While the circuit of Fig. 9 may not itself turn out to be practical, it illustrates that the device can provide enough output information to make at least a first-order distinction between the signal and offset.

REFERENCES

1. J. L. Moll, M. Tanenbaum, J. M. Goldey, and N. Holonyak, Proc. IRE *44* 1956, p. 1174.
2. I. M. Mackintosh, Proc. IRE, *46*, 1958, p. 1229; F. E. Gentry, F. W. Gutzwieler, N. H. Holonyak, and E. E. Von Zastrow, *Semiconductor Controlled Rectifiers*, Englewood Cliffs, N. J., Prentice-Hall 1964.
3. N. C. Voulgaris and Edward S. Young, IEEE Trans. Electron Devices, *ED-16*, 1969, p. 468; IEEE Journal of Solid State Circuits, *SC-5*, 1970, p. 146.
4. A. M. Barnett, IBM Journal of Res. and Dev., *13*, 1969, p. 522.
5. I. J. Saunders, Solid State Electr., *11*, 1968, p. 1165.
6. D. J. Bartelink and G. Persky, "Magnetic Sensitivity of a Distributed Si Planar PNPN Structure Supporting a Controlled Current Filament," to be published.
7. G. Persky and D. J. Bartelink, J. Appl. Phys., *42*, 1971, p. 4414.
8. Philip M. Morse and Herman Feshback, *Methods of Theoretical Physics*, New York: McGraw-Hill, 1953, p. 857.
9. D. J. Bartelink, G. Persky, and D. V. Speeney, Proc. IEEE, *59*, August 2, 1970, p. 318.
10. S. M. Sze, *Physics of Semiconductor Devices*, New York, Wiley-Interscience, 1969, p. 106.
11. J. B. Flynn, J. Appl. Phys., *41*, 1970, p. 2750.